

European summer climate variability in a heterogeneous multi-model ensemble

P.L. Vidale, D. Lüthi, R. Wegmann, C. Schär

Institute for Atmospheric and Climate Science, ETH Zürich, Switzerland

submitted 7 January 2005

revised 20 December 2005

In final form 31/07/2006

P. L. Vidale, Institute for Atmospheric and Climate Science ETH, Zürich, Switzerland, now at the NCAS Centre for Global Atmospheric Modeling, Earley Gate, University of Reading, Reading, RG6 6BB, UK, p.l.vidale@reading.ac.uk

Abstract. Recent results from an enhanced greenhouse-gas scenario over Europe suggest that climate change might not only imply a general mean warming at the surface, but also a pronounced increase in interannual surface temperature variability during the summer season (Schär et al. [2004]). It has been proposed that the underlying physical mechanism is related to land surface-atmosphere interactions. In this study we expand the previous analysis by including results from a heterogeneous ensemble of 11 high-resolution climate models from the PRUDENCE project. All simulations considered comprise 30-year control and enhanced greenhouse-gas scenario periods. While there is considerable spread in the models' ability to represent the observed summer variability, all models show some increase in variability for the scenario period, confirming the main result of the previous study. Averaged over a large-scale Central European domain, the models simulate an increase in the standard deviation of summer mean temperatures between 20 and 80%. The amplification occurs predominantly over land points and is particularly pronounced for surface temperature, but also evident for precipitation. It is also found that the simulated changes in Central European summer conditions are characterized by an emergence of dry and warm years, with early and intensified depletion of root-zone soil moisture. There is thus some evidence that the change in variability may be linked to the dynamics of soil-moisture storage and the associated feedbacks on the surface energy balance and precipitation.

1. Introduction

A full description of a climate state requires consideration of variability over a broad range of time scales, from centennial to intra-seasonal. Interannual variations represent a highly critical factor in terms of climate impacts. In Europe, for instance, society and agricultural production are adapted to a summer climate with small interannual variations, amounting to a mere 1K, while winter variability is much larger, with standard deviations up to and beyond 3K (Scherrer et al. [2005]). A hypothetical increase in interannual summer variability, for instance associated with climate change, might have a detrimental impact upon societal adaptation. The dramatic economic and societal repercussions of the extreme European summer of 2003 clearly demonstrate this kind of sensitivity (Schär and Jendritzky [2004]; Black et al. [2004]).

Analysis of previous literature suggests that the representation of mid-latitude summer interannual variability in climate models is a difficult topic. Recent studies (Collins et al. [2001]; Räisänen [2002]; Giorgi [2002]) indicate a tendency of current models to overestimate interannual surface temperature variability during the extra-tropical summer season. Some considerable differences in variability also exist between the CRU surface-temperature analysis (New et al. [2000]) and the corresponding ERA-40 reanalysis fields (Simmons et al. [2004]): the model-based reanalysis (ERA-40) overestimates the observed (CRU) variability (see section 3.1.2). These results somewhat contrast with an analysis of early GCM simulations over North America by Mearns et al. [1990], who found that most models suffered from a serious underestimation of observed interannual summer variability. The extent to which this change in overall bias is due to differences in the simulation of planetary-scale variability or due to changes in model physics is not known.

It is likely that the aforementioned model uncertainties are at least partly related to the representation of land-surface processes in general, and the soil-moisture precipitation feedback in particular (for recent reviews, see Betts [2004]). The feedback relies on a complex series of processes that involves soil-moisture conditions, the availability of moist static energy in the boundary layer and both short-wave and long-wave radiative processes, including their interaction with atmospheric humidity and clouds (see Betts et al. [1996], Eltahir [1998], and Schär et al. [1999]), all relevant for the occurrence of heat waves and droughts. Aspects of the soil-moisture-precipitation feedback loop have also been investigated in the context of climate change studies, motivated by the pioneering study of Wetherald and Manabe [1995] on droughts induced by greenhouse gas forcing. Seneviratne et al. [2002] demonstrate that simple first-generation bucket-type land-surface schemes overestimate the drying of the soil in summer in response to climate-change forcing, a result consistent with the tendency of earlier climate models to dry out too quickly. More recently, Hirschi et al. [2005] found that PRUDENCE models (Christensen et al. [2002]), all equipped with second generation land surface schemes, generally exhibit a rather realistic seasonal cycle of terrestrial water storage, but have a tendency to underestimate the amplitude of the seasonal water cycle. In a recent paper (Schär et al. [2004]), we downscaled climate change simulations with respect to European interannual variability during the summer season, using the CHRM regional climate model (Vidale et al. [2003]). Results suggest that, in response to greenhouse gas forcing, the European summer climate may not only experience a pronounced warming, but also a substantial increase in interannual variability, amounting to an increase of the standard deviation of summer temperatures by up to a factor two. Further analysis of our simulations suggests that the

mechanism behind the increase in variability may be tied to the occurrence of (partial) soil moisture depletion, which increases the Bowen ratio and thereby the conversion of net surface radiation into sensible heating, at the expense of evapotranspiration.

It is evident that the multitude of physical processes described above depends upon parameterized model physics. Lenderink et al. [2006] analyze the PRUDENCE simulations with regard to the surface energy budget, finding considerable sensitivity with respect to model formulation, for instance regarding the representation of downward long-wave radiation at the Earth's surface. The aforementioned studies are thus indicative of the potential for adding new insights to the investigation of climate change by considering processes in a broad range of model formulations.

The main purpose of the current study is to conduct a detailed model intercomparison and focus on the representation of summer interannual variability for current and scenario conditions. We make use of a total of 11 high-resolution models (both AGCMs and RCMs) from PRUDENCE, a project that investigated the uncertainties involved in estimating climate change and its impacts over Europe (Christensen et al. [2002], Christensen and Christensen [2006], Déqué et al. [2005], Déqué et al. [2006], Jacob et al. [2006]). In addition to land-surface processes and feedbacks, we will address the role of large-scale circulation anomalies during the summer season, as changes in the frequency of anticyclonic forcing represent an alternative hypothesis to explain changes in interannual variability. Such variability may be linked to monsoonal circulations by teleconnections (e.g. Rodwell and Hoskins [2001]), and there is also some indication that the recent trends in summer synoptic-scale circulation are consistent with climate change scenarios (Pal et al. [2004], Meehl and Tebaldi [2004]). However, as the PRUDENCE archive restricts atten-

tion mostly to surface fields, the corresponding analysis of synoptic activity is limited to one single RCM.

The outline of the paper is as follows: in section 2, the modeling approach is introduced; section 3 discusses the models' climatology, including their ability to represent current climate variability; finally, section 4 provides conclusions and an interpretation of the mechanisms uncovered by the intercomparison.

2. Methods

At the top of the PRUDENCE model hierarchy (see Christensen and Christensen [2006], this issue), fully coupled transient AOGCM simulations (e.g. Pope et al. [2000], Déqué et al. [2005]) were used to generate results that were ingested by atmosphere-only GCMs in time-window mode (e.g. Johns et al. [2003]), for the periods 1960-1990 (control, CTL) and 2070-2100 (scenario, SCN). The respective lateral boundary conditions (with a grid spacing of circa 200km), the SST and sea-ice distributions, but also initial conditions such as soil moisture and soil temperature, were in turn used by a number of RCMs for downscaling over Europe, with a targeted grid spacing of around 50 km. SSTs for the scenarios were obtained by applying a delta-change method (Pope et al. [2000] and Jones et al. [2001]) to the low-resolution AOGCM results. This procedure retains the SST variability at the level of the CTL experiment.

2.1. Setup of the regional downscaling experiments: CHRM

The CHRM RCM (Vidale et al. [2003]) is a state-of-the-art Regional Climate Model, using a regular latitude/longitude grid (0.5° by 0.5°) with a rotated pole and a hybrid sigma-pressure vertical coordinate. The model has been thoroughly tested in the past

and validated regarding its ability to represent current climate variability in response to large-scale forcing (Lüthi et al. [1996], Vidale et al. [2003]). Additional validation of the CHRM model, in regards to the water cycle, is available in Frei et al. [2003], Kleinn et al. [2005], Hirschi et al. [2005], Hohenegger and Vidale [2005], and papers in this issue of *Climatic Change*. All CHRM experiments presented in this study use the model configuration and physics, presented in Vidale et al. [2003] as version 2.3, and the same standard European domain. The integrations were forced at the lateral boundaries with data from two HadAM3 simulations (see Table 1) and comprise the periods 1960-1990 and 2070-2100 (SRES A2 scenario, Nakićenović et al. [2000]). The first year of each experiment was considered as spin-up and discarded, as was done by all other PRUDENCE partners.

Validation of 1961-1990 climate simulations is based on 0.5° data extracted from the Climatic Research Unit analysis (New et al. [2000]), as well as ERA-40 reanalysis (Simmons et al. [2004]). Some comparisons are also provided with an ERA-40 CHRM downscaling experiment, which spanned the 1958-2001 period (here analyzed for the overlapping period exclusively). All model data were processed at monthly intervals and interpolated to the standard CRU grid for intercomparison purposes.

2.2. Other models composing the heterogeneous ensemble

The PRUDENCE models used in this study include 3 GCMs (HadCM3, Arpege, ECHAM4) and 9 RCMs (mostly using HC data and an A2 scenario, see Table 1). The skill of these models at representing climate and its variability has also been considered in previous publications (Kjellström et al. [2005], Hagemann et al. [2004], Christensen et al. [1997]) and in this issue (Jacob et al. [2006], and Lenderink et al. [2006]). Some special model configurations require additional description: first, the driving AOGCM was run to

generate three ensemble members, and some institutions (CNRM, DMI and Hadley Centre) conducted higher-resolution simulations from these, using AGCMs or RCMs. Second, DMI conducted simulations using both the standard experiment and a similar A2/CTL scenario, using forcing data from an alternative AGCM, namely the MPI ECHAM4 model (Roeckner et al. [1996]), imposing the same base SSTs as the other GCMs. Third, the Arpege model (Déqué et al. [1998]) is a variable-resolution AGCM: it uses the SST and sea-ice distribution from HadCM3, but not the atmospheric lateral boundary conditions.

2.3. Analysis of interannual variability

For distributions described by large data samples (such as daily data), non-parametric quantile-based estimators – for instance the inter-quartile range – are more robust than parametric approaches (Ferro et al. [2005]). However, for small data samples (such as seasonal mean temperature), moment-based methods are superior, due to their higher statistical efficiency (Scherrer et al. [2005]). We therefore express interannual surface temperature variability in terms of its standard deviation for the 1961-1990 and 2071-2100 periods, assuming a Gaussian behavior.

An additional difficulty in the estimation of intrinsic variability is due to the presence of trends in the time series (Schär et al. [2004]). In the case of surface temperature, these may arise in response to transient greenhouse gas forcing or natural variations. Scherrer et al. [2005] provide a quantitative assessment of the associated artificial inflation of variability. Assuming 30-year time series, a typical standard deviation of 1 K, and (rather large) temperature trends of 1 to 2 K $(30 \text{ y})^{-1}$, they find that the inflation factor amounts to between 1.04 and 1.16. Thus, ideally we should detrend the data prior to the computation of the standard deviation. However, since not all data were available as seasonal time

series, the standard deviation values for some of the models had to be obtained directly from the data repository, as provided by the PRUDENCE participants. We estimate that this implies an overestimation of variability changes by typically 5 to 10%.

3. Results

3.1. Basic validation

3.1.1. Seasonal means.

The evaluation of seasonal means for CTL and SCN experiments in PRUDENCE is presented in companion papers by Jacob et al. [2006] and Christensen and Christensen [2006]. Here we introduce a CHRM-specific subset of that analysis, relevant to the specific objectives of the current study.

The CHRM model results are shown in 4-panel plots (e.g. Fig. 1), one for each season, in which we compare results of the CHRM model as driven by Hadley Centre (HC) data (top right) and by ERA-40 data (bottom right). The left-hand panels of each plot show the observational data from the CRU analysis (top) and the ERA40 re-analysis (bottom). Figure 1 shows that the model reproduces the main characteristics and location of precipitation maxima, together with climatological gradients. For winter, comparison of the four panels shows that the simulation captures the key features of the European climate with notable accuracy. For summer, comparison between ERA-40 and HadAM3-driven simulations shows that the simulation driven by HadAM3 has a tendency for a more pronounced Mediterranean dryness, which also extends further northward than in the ERA40-driven simulation. The dry bias over the Alps, already discussed in Vidale et al. [2003], is present in both simulations. In that study it was shown that the typical magnitude of precipitation biases was smaller than 1mm/day in most of the domain.

Figure 2 (left) indicates that the model also represents the surface (2m) temperature adequately, indeed correcting some of the winter (Spain, cold) and summer (SE Europe, warm and dry) biases that appeared previously in ERA-15 driven simulations (see Vidale et al. [2003], figures 2-3). The overestimation of temperatures in the Mediterranean and the Danube region appears to be more prominent in the HC-driven simulation than in the ERA40-driven simulation, but the representation of near-surface temperature over southern Spain region appears more realistic in the HC-driven simulation. This summer temperature bias and its geographical distribution have also been discussed recently in Hohenegger and Vidale [2005] and appear to be in part related to the specification of aerosols.

3.1.2. Interannual variability.

Interannual variability, expressed as the standard deviation of the seasonal means for the 1961-1990 and 2071-2100 periods, will be presented in the following sections for all models participating in the intercomparison (see section 2 for methodological details). For surface temperature, the CHRM credibly represents the pronounced differences between the seasons, with substantially larger variability in the winter season (not shown). For the summer season, Fig. 2 (right-hand plot) shows that both CHRM simulations represent some of the observed west-east gradient, but in general there is a considerable overestimation of interannual variability. It can also be noted that there are large differences in the representation of interannual variability between the CRU and the ERA-40 reanalysis. The overestimation by CHRM amounts to about 25%, especially in the southern part of the domain. A more pronounced discrepancy is found between HC-driven and ERA40-driven simulations in the Danube basin, a region for which in particular the

ERA40-driven simulation shows an anomalous pattern of high variability (up to 1.5 K) during the summer season.

In order to intercompare all participating models in a single diagram, we focus now on the spatial average of the interannual variability (standard deviation) over the land-points of a large Central European area (3W-27E and 44N-55N) that is marked as a red box in Fig. 2 (top-right). Figure 3 combines the summer variability of precipitation (ordinate) with the variability of surface temperature (abscissa). It is immediately evident from this plot that there is a large spread between the different models, with the simulated standard deviation ranging between 0.5 and 1.4°C. Also, there is some degree of discrepancy between the two observational data sets from the ERA-40 reanalysis and the CRU analysis (data points 17 and 19, respectively). Most models overestimate the interannual variability with respect to the CRU analysis, and there is also some correlation between the overestimation of temperature and precipitation variability. The KNMI and CHRM models driven by HadAM3 (data points 12 and 6, respectively) yield values that are close to the ERA-40 reanalysis (about 0.9°C in temperature and 0.7 mm/day in precipitation). Results from other models in the consortium indicate that the HadAM3 lies at the low end, while the HadRM3 is at the high end of the variability range. Different realizations of each model tend to cluster (e.g. DMI or CNRM), while results from independent models appear to be further from each other. For instance, the results from the DMI model driven by ECHAM4 (data point 16) are positioned near those of the other two DMI simulations driven by HadAM3 (data points 1 and 2). The clustering of data points suggests that the representation of physical processes is a key factor in determining the interannual variations of summer surface temperature. Indeed, differences in parameterizations between

RCMs appear more important than differences in synoptic climatology between AGCMs, at least for the sample of models considered in Figure 3.

3.2. Changes in interannual variability

Changes in mean climate for PRUDENCE models were discussed in Christensen and Christensen [2006] (this issue); for CHRMs, summer results were presented in Schär et al. [2004]. We turn to changes in variability. Figure 4 shows a map of the change in interannual variability, by season, between the two simulation periods (SCN-CTL) for the ensemble mean of all models listed in Table 1. By comparing the four panels, it is immediately evident how the change in variability is limited to JJA, while for all other seasons the ensemble shows no change or even a moderate variability decrease. Having identified the boreal summer as a key season for European climate change and in order to assess the range of responses in the ensemble, we expand the analysis with a selection of six maps of JJA temperature variability change, shown in figure 5. Both figures 4 and 5 show that the pattern of change in JJA variability presented in Schär et al. [2004] is reproduced by other PRUDENCE models, but in a less consistent fashion than was the case for the changes in the mean (see also Christensen and Christensen [2006]). The results in figures 4 and 5 indicate that the location of pronounced increases in surface temperature variability is a) mostly limited to land-surfaces; b) not co-located with the region of maximum mean change (Mediterranean); but c) near the region of maximum horizontal gradient in mean change (Central Europe); and d) mostly positive. The DMI models stand out at the low end of the range of variability change, while the KNMI and HadAM3 are at the high end. The CNRM model (representing an independent AGCM using the same SST scenario) shows changes in variability that are rather similar to those of the HadAM3-driven RCMs,

except over the Mediterranean Sea. The DMI model driven by HadAM3 has a maximum change in variability further south than the other models (in Northern Spain and Southern France). The same model, when driven by ECHAM4 data (not shown in Fig. 5, but present in Fig. 6), shows a similar, but even smaller change in variability, although still exhibiting an increase in interannual variability by about 40% over most of France. Comparison of other RCM simulations using different HadAM3 ensemble members as driving data (not shown) indicates a high level of consistency.

By reference to the analysis in 3.1.2, we introduce a second general scatter plot, with the results of 11 of the models in the PRUDENCE consortium. Figure 6 summarizes the information in Fig. 5, by showing area average relative changes in variability over Central Europe, with temperature changes on the abscissa and precipitation changes on the ordinate. All model simulations reflect an increase in temperature variability, but to a different extent. The CHRМ model, with about 60% increase in the case of temperature and 10% increase in the case of precipitation, is at the center of the distribution, while the HC models are at the two extremes, with the GCM on the higher end and the RCM on the lower end (together with the second GCM ensemble member). Some models (e.g. HadAM3 and CNRM) show large changes in T_{2m} standard deviation, over 80%, while some others (e.g. HadRM3 and HadAM3 from the second ensemble member) show the least change, about 30%. Again, as in Fig. 3, there is some correlation between variability changes in temperature and precipitation. Model formulation seems to matter, as shown by the results from the two DMI simulations and the three CNRM ensemble members, which cluster despite using different driving GCMs or different SSTs, respectively. Overall, the change in temperature variability is in the 0-90% range, while the change in

precipitation variability is more contained, between -10 and 40%. Regarding the change in interannual variability of precipitation, it should be noted that the latter is accompanied by a decrease in mean precipitation over the analysis domain for all models considered (Christensen and Christensen [2006]). The coefficient of variation (the standard deviation normalized by the mean, not shown) thus exhibits a substantially stronger increase in relative precipitation variability. This might be relevant for impact studies, as the coefficient of variation is the more appropriate indicator for water resource management purposes.

3.3. Processes involved in change of variability

Having seen how the change in temperature variability is distributed in space and how it depends on model formulation, we consider the underlying physical processes. To this end, we turn to an analysis of temperature, precipitation and soil moisture anomalies with respect to the 1961-1990 (CTL) means. We present plots of area-averaged values over the same Central European region presented above, for both control and scenario simulations.

3.3.1. Precipitation anomalies.

The first set of plots (Fig. 7) presents precipitation/temperature anomalies, similar to what was introduced in Schär et al. [2004]. The blue points correspond to anomalies produced by the individual summers of the CTL experiment, while red points correspond to anomalies produced by the SCN experiment. All models show a marked shift towards a warmer and drier climate, as the two clouds of points are well separated. At the same time there is an increase in variability, illustrated by the larger spread in the red cloud. The same plots also show that there appears to be a change in the slope of the linear regression line belonging to each cloud, indicating a shift in conditions: a larger variability of precipitation (relative to temperature) in current climate gives way to a

comparatively larger variability of temperature in the scenario. In addition, the plots convey information about the diurnal cycle, by including data points corresponding to the 2m minimum (triangles pointing downwards) and maximum (triangles pointing upwards) temperatures. The data show how drier years display a broadening of the diurnal cycle, with maximum temperatures being responsible for more of the change in drier years. This result is consistent with a recent analysis of Kjellström et al. [2005], and points to mechanisms associated with the diurnal cycle. This suggests that we should also consider soil moisture anomalies, as the latter can potentially link the surface radiation balance (thus temperature) and plant physiology to precipitation, through evapotranspiration.

3.3.2. Soil moisture anomalies. Plots of JJA temperature (abscissa) versus soil moisture (ordinate) in Fig. 8 indicate that indeed the climate change signal is revealed as a shift towards warmer and drier climates (in terms of soil moisture), characterized by enhanced exploitation of soil moisture reservoirs by vegetation. The decrease in soil moisture levels is the result of decreasing growing season precipitation and increasing plant transpiration, that is, the conversion of increased net surface radiation into latent rather than sensible heat flux. As was the case with precipitation and temperature, there is a distinct separation in the two clouds of points, an apparent change in slope of the regression line, and a broadening of the distribution of soil moisture in a warmer climate. In comparison to the temperature-precipitation diagrams (Fig. 7) there is a much larger heterogeneity in model response, which is connected with individual model formulations (e.g. total depth of soil, water retention capabilities etc.). The shapes of the red clouds, which tend to flatten and broaden in correspondence to the lowest soil moisture levels, indicate that some models may lack the ability to represent a full seasonal cycle

in conditions of extremely high summer temperatures, possibly because they are running out of water early in the growing season.

3.3.3. Soil moisture seasonal cycle. For each of the two simulation periods (CTL, SCN) we plot in Fig. 9 the mean root-zone soil water cycles of the Central European area used in previous sections. The interannual variability is indicated by the thin upper and lower lines, which mark one standard deviation from the means. Current climate is represented in blue and scenario climate in red. A large disparity among models, even under current climatic conditions, exists. Hirschi et al. [2005], using the methodology of Seneviratne et al. [2004], have shown that a reasonable annual soil moisture cycle for this Central European region should have an amplitude of around 100 mm. For current climatic conditions, some models have trouble representing this amplitude. From the point of view of climate change, it is to be expected that the soil moisture cycle should change due to: a) higher winter precipitation; b) lower summer precipitation; c) higher summer evapotranspiration in response to increases in net surface radiation; and d) longer growing season, which implies more use of soil moisture for photosynthesis. The simulations meet some of these expectations. For instance, there is evidence that during spring the root-zone soil water is accessed at an earlier date and at a faster rate than in current climatic conditions, so that a late summer deficit is indeed evident in most of the plots. Most of the models show, despite a winter recharge similar or above current climate levels (evident especially for CNRM and HC), distinctly lower values of soil moisture at the peak of summer each year (typically a 40 mm deficit), and a distinct delay in the fall recharge.

Some models (e.g. the DMI model) show little change in winter soil water levels (despite the enhanced soil water cycle), while other models exhibit an increase of the winter soil

water level (e.g. CNRM). In particular, the KNMI model stands out (having a much deeper soil and larger water reservoirs than the other PRUDENCE models) in that the current and scenario water cycles are clearly separated from each other, despite small changes in the amplitude of the seasonal water cycle. This model also shows a particularly large associated change in temperature variability (see Fig. 5).

3.3.4. Large-scale circulation changes.

Here we briefly consider changes in synoptic-scale atmospheric circulation during the summer season according to the CHRM model, in order to obtain a more complete picture of involved mechanisms. Maps of changes in the mean surface pressure (Fig. 10, top left) indicate a simulated summer increase of 2hPa over the NW portion of the domain. The surface pressure change is accompanied at higher levels by corresponding changes in geopotential height. Geopotential height at 500 hPa (Fig. 10, bottom left) is higher over the entire domain for the SCN simulation in response to the mean warming, and this effect is most pronounced over the west of the domain, where a well-defined ridge pattern is visible. The accompanying standard deviation field (bottom right, computed from seasonal means) shows that the change in interannual variability at 500 hPa consists of a positive anomaly of up to 16 m, located over and downstream of the area with large changes in surface temperature variability (compare with Fig. 6). A map of change in the mean temperature at 850 hPa (Fig. 10, top right) between current and scenario climate indicates that the mean summer temperature is warmer by over 5K all throughout the boundary layer in the southern part of the domain, and that this signal is also present over much of the Mediterranean sea. The complementary map for the change in standard deviation of 850 hPa temperature (not shown) reveals a pattern almost exactly coincident

in area and shape with that over the same region at the surface (Fig. 6). These results are indicative of some degree of interplay between local thermodynamics and the larger-scale circulation imposed by the driving GCM. In order to assist with the interpretation of these summer results, it is worth mentioning that similar anomalies, albeit of opposite sign, are present during the winter season (not shown). Circulation changes associated with the aforementioned anomalies are expected to cause local winds to be more westerly in the winter (bringing more oceanic humidity to the continent) and easterly in the summer and fall, reducing moist advection from the west. These changes in surface winds have indeed been shown to be a characteristic of the HadAM3-driven A2 scenario simulation over Central Europe, as discussed in Ulden and Lenderink [2006] and are fully consistent with the increase in winter precipitation seen in all PRUDENCE models.

4. Discussion and Conclusions

The PRUDENCE climate change experiments have shown considerable agreement among participating models. For winter, there is increasing precipitation in Central Europe, accompanied by a pronounced warming in the more continental north-eastern regions of the European continent (see Christensen and Christensen [2006]). For summer, a rather dramatic shift to warmer and drier conditions, especially in the southern portion of Europe, has been a common feature emerging from the above analysis. The change in variability has been shown to be a feature of Central Europe, located near the maximum N-S gradient of mean temperature change, and is simulated during the summer season only. However, while all models considered show some increase in variability, supporting what has been shown in our previous paper (Schär et al. [2004]), uncertainty and disagreement remain between models regarding the amplitude of the effect and the geographical

location of the variability changes. Several mechanisms have been invoked to explain the change in variability: changes in large-scale synoptic forcing and storm track dynamics (e.g. Meehl and Tebaldi [2004]), and/or changes in local physics, involving alterations to the hydrological cycle and the surface energy balance (e.g. Schär et al. [2004]).

The key result of our intercomparison, in terms of local physics, is that SCN soil moisture reservoirs are accessed earlier by the models during the spring, resulting in a peak summer deficit. In fact, an earlier and longer-lasting growing season, coexisting with warmer and drier SCN summers, activates plant physiology and transpiration for a longer period of time and requires an earlier and more intensive use of soil water. This phenological interpretation is consistent with results from a 20-year observational study conducted over Europe (Stöckli and Vidale [2004]). At the peak of summer, warmer and drier conditions are more likely, consistent with an enhanced soil moisture-precipitation feedback, as was shown in Figs. 7 and 8, also revealed by the correlation between mean change and relative change in the anomalies. For the means, this correlation has been amply discussed in the past (e.g. Allen and Ingram [2002]) in terms of energy availability, but this argument applies more to winter; for our summer cases a reduction in surface evaporation is the controlling mechanism, despite a surplus in net available energy. Further confirmation that land surface processes are intimately involved in the composition of variability comes from the analysis of model diurnal temperature range ($T_{max} - T_{min}$), which is generally broader in warmer/drier years. In models, this kind of behavior increases the probability of hitting thresholds at which no more water is available for transpiration (wilting point), so that plant activity will cease, creating negative correlations between soil-water levels and temperatures, as well as precipitation. In the extreme, the occurrence of a biophysical

runaway process, often referred to as "stomatal suicide", is more likely than under current climatic conditions. These dry spells could potentially be interrupted by synoptic-scale weather events, which however tend to be less frequent in the scenario climate, with a marked shift of Mediterranean-type summer conditions towards the north. This also explains the changes in variability.

Why do we see such a heterogeneous response in plots of change in variability? The chain of processes outlined above suggests that two classes of models may underestimate variability: (a) models with a too weak soil moisture memory, leading to drought-like effects even in current climate summers; and (b) models with a too strong soil moisture memory, lacking a drought potential under current climatic conditions. In general, as the seasonal cycle of soil moisture depends on a wide number of parameterizations (among them atmospheric radiation, cloud-radiation interactions, runoff formation, transpiration, etc), it is not feasible to ascribe a particular model failure to one particular parameterization scheme. However, the first condition (a) may be associated with too shallow and easily depleted soils, creating an evapotranspiration deficit, so that surface temperatures will reflect an almost direct conversion of net radiation into sensible heat. This type of model is not capable of sustaining the seasonal soil moisture cycle and most summers will resemble each other because of a local collapse of the hydrological cycle. The second condition (b) may be associated with models that have either too large a soil moisture reservoir initially (else provide too easy access to deep soil water) or that are tuned to limit their water uptake during the earlier and warmer spring, despite favorable conditions for vegetation. Such formulations may be able to artificially sustain exceptionally cool and moist summers, under current and future climatic conditions.

Models displaying strong relative increases of summer temperature variability are either those with too low variability in current climate (e.g. CNRM), so that even small absolute changes have a considerable weight in the relative change, or models which never fully reach the wilting point. Models in the latter group are capable of responding to a wider range of environmental conditions, possibly as a result of adapted plant physiology (larger tolerance to high temperature regimes), or of employing soils with a deeper root zone. For instance, the KNMI model reproduces current climate variability quite accurately (being near the center of Fig. 3) and produces strong relative variability changes (about 90%), while exhibiting a seasonal hydrological cycle active enough to delve deeply into the abundant soil reservoirs (see Figs. 8 and 9). This may be showing that a climate model, given more degrees of freedom, may tend to produce an even larger range of responses to climate change than a model specifically designed for current climatic conditions. This hypothesis, however, should be tested by configuring an independent model with a soil layer distribution similar to that used by KNMI and running sensitivity experiments, something not feasible in the present context.

Finally, in addition to local thermodynamic, hydrological and radiative changes, changes in surface temperature variability are also affected by large-scale circulation changes. Our study was unable to rigorously quantify the relative contributions. However, many climate change simulations show a ridging over Western Europe, which suggests an increase in the incidence of warm summers. There is also an increase in 500 hPa geopotential height variability. This signal is noteworthy, but located downstream from that of increases in surface temperature variability, thus possibly a consequence (rather than the origin) of the simulated increases in variability.

Acknowledgments.

This research was supported by the Fifth Framework Programme of the European Union (project PRUDENCE, contract EVK2-2000-00132), by the Swiss State Secretariat for Education and Research (BBW contract 01.0305-1), and by the Swiss National Science Foundation (NCCR Climate). We wish to acknowledge the help and support of Mark Linger (MeteoSwiss, Zürich) in obtaining ERA40 analysis and of Ole B. Christensen, (DMI Copenhagen), for managing the PRUDENCE OpenDAP server. The model simulations were performed at the ETH supercomputer centers in Zürich, with support provided by Bruno Loepfe; and at CSCS Manno (Ticino), with support from Angelo Mangili, Claudio Redaelli and Francesco Benvenuto.

References

- M.R. Allen and W.J. Ingram. Constraints on future changes in climate and the hydrologic cycle. *Nature*, 419(doi:10.1038/nature01092):224–232, 2002.
- A.K. Betts. Understanding hydrometeorology using global models. *Bull. Amer. Meteorol. Soc.*, 85(11):1673–1688, 2004.
- A.K. Betts, J.H. Ball, A.C.M. Beljaars, M.J. Miller, and P.A. Viterbo. The land-surface atmosphere interaction: A review based on observational and global modeling perspectives. *J. Geophys. Res.-Atmos.*, D101:7209–7225, 1996.
- E. Black, M. Blackburn, G. Harrison, B. J. Hoskins, and J. Methven. Factors contributing to the summer 2003 European heatwave. *Weather*, 59(8):217–223, 2004.
- J.H. Christensen, T. R. Carter, and F. Giorgi. PRUDENCE employs new methods to assess European climate change. *EOS*, 83:147, 2002.

- J.H. Christensen and O.B. Christensen. A summary of the PRUDENCE model projections of changes in European climate during this century. *Climatic Change*, Submitted, 2006.
- J.H. Christensen, B. Machenhauer, R.G. Jones, C. Schär, P.M. Ruti, M. Castro, and G. Visconti. Validation of present-day regional climate simulations over Europe: LAM simulations with observed boundary conditions. *Climate Dynamics*, 13:489–506, 1997.
- O.B. Christensen, J.H. Christensen, B. Machenhauer, and M. Botzet. Very high-resolution regional climate simulations over Scandinavia—Present climate. *J. Climate*, 117:3204–3229, 1998.
- M. Collins, S. F. B. Tett, and C. Cooper. The internal climate variability of HadCM3, a version of the Hadley Centre coupled model without flux adjustments. *Climate Dynamics*, 17(1):61–81, 2001.
- M. Déqué, R. G. Jones, M. Wild, F. Giorgi, J. H. Christensen, D. C. Hassell, P. L. Vidale, B. Röckel, D. Jacob, E. Kjellström, M. de Castro, F. Kucharski, and B. van den Hurk. Global high resolution versus limited-area model scenarios over Europe: results from the PRUDENCE project. *Climate Dyn.*, 25(doi:10.1007/s00382-005-0052-1):653–670, 2005.
- M. Déqué, P. Marquet, and R.G. Jones. Simulation of climate change over Europe using a global variable resolution general climate model. *Climate Dynamics*, 14:173–189, 1998.
- M. Déqué, D. Rowell, D. Lüthi, F. Giorgi, J. H. Christensen, B. Rockel, D. Jacob, E. Kjellstrom, M. de Castro, and B. van den Hurk. An intercomparison of regional climate models for Europe: assessing uncertainties in model projections. *Climate Dyn.*, submitted, 2006.

- E. A. B. Eltahir. A soil moisture-rainfall feedback mechanism. part 1: Theory and observations. *Water Resour. Res.*, 34:765–776, 1998.
- C.A.T. Ferro, D. B. Stephenson, and A. Hannachi. Simple non-parametric techniques for exploring changing probability distributions of weather. *J. Climate*, in press, 2005.
- C. Frei, J.H. Christensen, M. Déqué, D. Jacob, R.G. Jones, and P.L. Vidale. Daily precipitation statistics in regional climate models: Evaluation and intercomparison for the European Alps. *J. Geophys. Res. – Atmos.*, 108(D3):Art. No. 4124, 2003.
- F. Giorgi. Variability and trends of sub-continental scale surface climate in the twentieth century. Part II: AOGCM simulations. *Climate Dyn.*, 18(8):693–708, 2002.
- S.B. Hagemann, B. Machenhauer, O.B. Christensen, M. Déqué, D. Jacob, R.G. Jones, and P.L. Vidale. Evaluation of water and energy budgets in regional climate models applied over Europe. *Climate Dynamics*, 23(DOI 10.1007/s00382-004-0444-7):547–567, 2004.
- M. Hirschi, S.I. Seneviratne, and C. Schär. Seasonal variations in terrestrial water storage for major mid-latitude river basins. *J. Hydrometeor.*, in press, 2005.
- C. Hohenegger and P.L. Vidale. Sensitivity of the European climate to aerosol forcing as simulated with a regional climate model. *J. Geophys. Res.-Atmos.*, 110(D6):Art. No. D06201, 2005.
- M. Hulme, G. Jenkins, X. Lu, J.R. Turnpenny, T.D. Mitchell, R.G. Jones, J. Lowe, J.M. Murphy, D. Hassell, P. Boorman, R. McDonald, and S. Hill. Climate change scenarios for the United Kingdom: the UKCIP02 scientific report. Technical report, Tyndall Centre for Climate Change Research, 2002.

- D. Jacob. A note to the simulation of the annual and inter-annual variability of the water budget of the Baltic Sea drainage basin. *Meteor. Atm. Phys.*, 77:61–73, 2001.
- D. Jacob, L. Bärring, O.B. Christensen, J.H. Christensen, M. de Castro, M. Déqué, F. Giorgi, S. Hagemann, M. Hirschi, R. Jones, E. Kjellström, G. Lenderink, B. Rockel, E. Sánchez, C. Schär, S.I. Seneviratne, S. Somot, A. van Ulden, and B. van den Hurk. An intercomparison of regional climate models for Europe: design of the experiments and model performance. *Climatic Change*, submitted, 2006.
- T.C. Johns, J. M. Gregory, W. J. Ingram, C. E. Johnson, A. Jones, J. A. Lowe, J. F. B. Mitchell, D. L. Roberts, D. M. Sexton, D. S. Stevenson, S.F.B. Tett, and M.J. Woodage. Anthropogenic climate change for 1860 to 2100 simulated with the HadCM3 model under updated emissions scenarios. *Clim. Dynamics*, 20:583–612, 2003.
- R.G. Jones, J.M. Murphy, D.C. Hassell, and R. Taylor. Ensemble mean changes in a simulation of the European climate of 2070-2100 using the new Hadley Centre regional modelling system HadAM3H/HadRM3H. Technical report, Hadley Centre Report, Hadley Centre, Exeter, UK, 2001, 2001. URL <http://prudence.dmi.dk>.
- R.G. Jones, J.M. Murphy, and M. Noguer. Simulation of climate change over Europe using a nested regional-climate model. I: Assessment of control climate, including sensitivity to location of lateral boundaries. *Q. J. R. Meteorol. Soc.*, 121:1413–1449, 1995.
- E. Kjellström, L. Bärring, D. Jacob, R. Jones, G. Lenderink, and C. Schär. Variability in daily maximum and minimum temperatures: Recent and future changes over europe. *Climatic Change*, submitted, 2005.
- J. Kleinn, C. Frei, J. Gurtz, D. L'uthi, P.L. Vidale, and C. Sch'ar. Hydrologic simulations in the Rhine basin driven by a regional climate model. *J. Geophys. Res. - Atmos.*, 110

(D4):Art. No. D04102, 2005.

D.M. Lawrence and J.M. Slingo. Weak land-atmosphere coupling strength in HadAM3:

The role of soil moisture variability. *J. Hydrometeorology*, in press, 2005.

G. Lenderink, B. van den Hurk, E. van Meijgaard, A. van Ulden, and H. Cuijpers. Simulations of present day climate in RACMO2: first results and model developments.

Technical Report TR-252, Royal Netherlands Meteorological Institute, 2003.

G.A. Lenderink, B. van Ulden, B. van den Hurk, and E. van Meijgaard. Summertime interannual temperature variability in an ensemble of regional model simulations: analysis of the surface energy budget. *Climate Dyn.*, submitted, 2006.

D. Lüthi, A. Cress, H.C. Davies, C. Frei, and C. Schär. Interannual variability and regional climate simulations. *Theor. Appl. Climatol.*, 53:185–209, 1996.

L.O. Mearns, S. H. Schneider, S. L. Thompson, and L. R. McDaniel. Analysis of climate variability in general-circulation models in comparison with observations and changes in variability in 2xCO₂ experiments. *J. Geophys. Res. Atmos.*, 95(D12):20469–20490, 1990.

G. A. Meehl and C. Tebaldi. More intense, more frequent, and longer lasting heat waves in the 21st century. *Science*, 305 (5687):994–997, 2004.

N. Nakićenović, J. Alcamo, G. Davis, B. de Vries, J. Fenhann, S. Gaffin, K. Gregory, A. Grübler, T.Y. Jung, T. Kram, E.L. La Rovere, L. Michaelis, S. Mori, T. Morita, W. Pepper, H. Pitcher, L. Price, K. Riahi, A. Roehrl, H.-H. Rogner, A. Sankovski, M. Schlesinger, P. Shukla, S. Smith, R. Swart, S. van Rooijen, Victor, N., and Dadi Z. *Emission scenarios. A special report of Working Group III of the Intergovernmental Panel on Climate Change*. Cambridge University Press, Cambridge, United Kingdom

and New York, NY, USA, 2000.

- M. New, M. Hulme, and P. Jones. Representing twentieth-century space-time climate variability. Part II: Development of 1901-96 monthly grids of terrestrial surface climate. *J. Climate*, 13:2217–2238, 2000.
- J.S. Pal, F. Giorgi, and X. Bi. Consistency of recent European summer precipitation trends and extremes with future regional climate projections. *Geophys. Res. Letters*, 31 (Art. No. L13202):doi:10.1029/2004GL019836, 2004.
- J.S. Pal, E. Small, and E. Eltahir. Simulation of regional-scale water and energy budgets: representation of subgrid cloud and precipitation processes within RegCM. *J. Geophys. Res.-Atmos.*, 105:29579–29594, 2000.
- D.V. Pope, M. Gallani, R. Rowntree, and A. Stratton. The impact of new physical parameterizations in the Hadley Centre climate model HadAM3. *Climate Dyn.*, 16: 123–146, 2000.
- J. Räisänen. CO₂-induced changes in interannual temperature and precipitation variability in 19 CMIP2 experiments. *J. Climate*, 15(17):2395–2411, 2002.
- J. Räisänen, U. Hansson, A. Ullerstig, R. Döscher, L.P. Graham, C. Jones, H.E.M. Meier, P. Samuelsson, and U. Willén. European climate in the late twenty-first century: regional simulations with two driving global models and two forcing scenarios. *Climate Dynamics*, 22:13–31, 2004.
- M.J. Rodwell and B. J. Hoskins. Subtropical anticyclones and summer monsoons. *J. Climate*, 14(15):3192–3211, 2001.
- E. Roeckner, K. Arpe, L. Bengtsson, M. Christoph, M. Claussen, L. Dümenil M. Esch, M. Giorgetta, U. Schlese, and U. Schulzweida. The atmospheric general circulation

- model ECHAM-4: model description and simulation of present-day climate. Technical Report 218, Max-Planck-Institute for Meteorology, Hamburg, Germany, 1996.
- E. Sanchez, C. Gallardo, M.A. Gaertner, A. Arribas, and M. Castro. Future climate extreme events in the Mediterranean simulated by a regional climate model: first approach. *Global and Planetary Change*, submitted, 2005.
- C. Schär and G. Jendritzky. Hot news from summer 2003. *Nature*, 432:559–560, 2004.
- C. Schär, D. Lüthi, and U. Beyerle. The soil-precipitation feedback: A process study with a regional climate model. *Journal of Climate*, 12:722–741, 1999.
- C. Schär, P.L. Vidale, D. Lüthi, C. Frei, C. Häberli, M.A. Liniger, and C. Appenzeller. The role of increasing temperature variability for European summer heat waves. *Nature*, 427(doi:10.1038/nature02300):332–336, 2004.
- S. C. Scherrer, C. Appenzeller, M.A. Liniger, and C. Schär. European temperature distribution changes in observations and climate change scenarios. *Geophysical Research Letters*, 32(19):Art. No. L19705, doi:10.1029/2005GL024108, 2005.
- S.I. Seneviratne, J. S. Pal, E. A. B. Eltahir, and C. Schar. Summer dryness in a warmer climate: a process study with a regional climate model. *Clim. Dyn.*, 20(1):69–85, 2002.
- S.I. Seneviratne, P. Viterbo, D. Luthi, and C. Schar. Inferring changes in terrestrial water storage using ERA-40 reanalysis data: The Mississippi River basin. *Journal of Climate*, 17(11):2039–2057, 2004.
- A.J. Simmons, P.D. Jones, V.D. Bechtold, A.C.M. Beljaars, P.W. Kållberg, S. Saari-
nen, S.M. Uppala, P. Viterbo, and N. Wedi. Comparison of trends and low-frequency variability in CRU, ERA-40 and NCEP/NCAR analyses of monthly-mean surface air temperature. *J. Geophys. Res.-Atmos.*, 109(D24):Art. No. D24115, 2004.

- J. Steppeler, G. Domus, U. Schättler, H.W. Bitzer, A Gassman, U Damrath, and G. Gregoric. Meso-gamma scale forecasts using the nonhydrostatic model LM. *Meteorol. Atmos. Phys.*, 82(1-4):75–96, 2003.
- R. Stöckli and P. L. Vidale. European plant phenology and climate as seen in a 20-year avhrr land-surface parameter dataset. *International Journal of Remote Sensing*, 25(17):3303–3330, 2004.
- A. Van Ulden and G. Lenderink. Circulation statistics in the PRUDENCE ensemble. *Climatic Change*, submitted, 2006.
- P. L. Vidale, D. Luthi, C. Frei, S. I. Seneviratne, and C. Schär. Predictability and uncertainty in a regional climate model. *J. Geophys. Res.-Atmos.*, 108:Art. No.–4586, 2003.
- R.T. Wetherald and S. Manabe. The mechanisms of summer dryness induced by greenhouse warming. *J. Climate*, 8:3096–3108, 1995.

List of tables

1. Climate models participating in PRUDENCE and used in this study

List of figures

Fig. 1: Mean 1961-1990 precipitation for winter (left) and summer (right) in mm/day. The four panels in each plot show CHRM simulations driven by the ERA-40 reanalysis (ERA40 CHRM) and the HC model chain (HC CHRM), along with an analysis of observational data (CRU), and results of a reanalysis (ERA40).

Fig. 2: 1961-1990 summer temperature as simulated by CHRM: mean (left) and standard deviation (right), in °C. The four panels in each plot are as in Fig.1. The red box on the top-right panel defines the region used for area averaging in subsequent analysis (land points only).

Fig. 3: Comparison of variability as simulated by PRUDENCE models for 1961-1990. Blue data points show domain-averaged values of the standard deviation of precipitation and 2m temperature for Central Europe in mm/day and K. The averaging domain is shown in Fig. 2. The green data point shows the CRU observations, the red points show the ERA-40 reanalysis and a CHRM simulation driven by ERA-40.

Fig. 4: Ensemble mean changes of the interannual variability of surface temperature for the four seasons, expressed as relative change $(SCN-CTL)/CTL$ of standard deviation in percent. All models in Table 1 are included.

Fig. 5: Changes in JJA interannual variability of surface temperature, expressed in percent. The panels show the results of six selected models/groups (from left to right and top to bottom): CHRM/ETH, CNRM/MeteoFrance, HIRHAM/DMI, HadAM3/HC, RACMO2/KNMI, RegCM/ICTP.

Fig. 6: As in Fig. 3, but showing the variability changes as simulated by PRUDENCE models, in percent.

Fig. 7: PRUDENCE simulated JJA temperature versus precipitation anomalies with respect to 1961-1990 means, for the same models as in Fig. 5, in K and mm/day. The three symbols show seasonal averages of minimum, mean and maximum temperatures.

Fig. 8: PRUDENCE simulated JJA temperature versus soil-moisture anomalies with respect to 1961-1990 means, for the same models as in Fig. 5, in K and mm.

Fig. 9: Mean yearly cycle of total soil moisture content in CTL (blue) and A2 scenario (red) experiments for the same models, as in Fig. 5, in mm. The thin lines above and under each thick line indicate the spread within the two 30-year periods, expressed in terms of the standard deviation.

Fig. 10: Changes in JJA synoptic-scale circulation, as simulated by the CHRM model (2071-2100 versus 1961-1990). Top left: change in mean MSL pressure (hPa); top right: change in mean 850hPa temperature (K); bottom left: change in mean 500 hPa height (m); bottom right: change in standard deviation of 500hPa height (m).

Table 1. PRUDENCE models used in this study ^a

Institution	Country	Model name	Simulation names	Scenario	Reference
CNRM	France	Arpege	DE4-DE8 (mem1)	HC-A2	Déqué et al. [1998]
			DE4-DE8 (mem2)	HC-A2	
			DE3-DE7 (mem3)	HC-A2	
DMI	Denmark	HIRHAM	HC1-HS1 (mem1)	HC-A2	Christensen et al. [1998]
			HC2-HS2 (mem2)	HC-A2	
			ECSCR-ECCTL	EC-A2	
ETH	Switzerland	CHRM	HC_CTL-HC_A2	HC-A2	Vidale et al. [2003]
GKSS	Germany	CLM	CTL-SA2	HC-A2	Steppeler et al. [2003]
Hadley Centre	UK	HadAM3	acdhd-acftc (mem1)	HC-A2	Hulme et al. [2002]
		HadAM3	acdhe-acftd (mem2)	HC-A2	
		HadRM3	achgi-ackda	HC-A2	
ICTP	Italy	RegCM	ref-A2	HC-A2	Pal et al. [2000]
KNMI	Netherlands	RACMO2	HC1-HA2	HC-A2	Lenderink et al. [2003]
MPI	Germany	REMO	3003-3006	HC-A2	Jacob [2001]
SMHI	Sweden	RCAO	HCCTL-HCA2	HC-A2	Räisänen et al. [2004]
UCM	Spain	PROMES	control-A2	HC-A2	Sanchez et al. [2005]

^a data extracted from the PRUDENCE OpenDAP server, <http://prudence.dmi.dk>

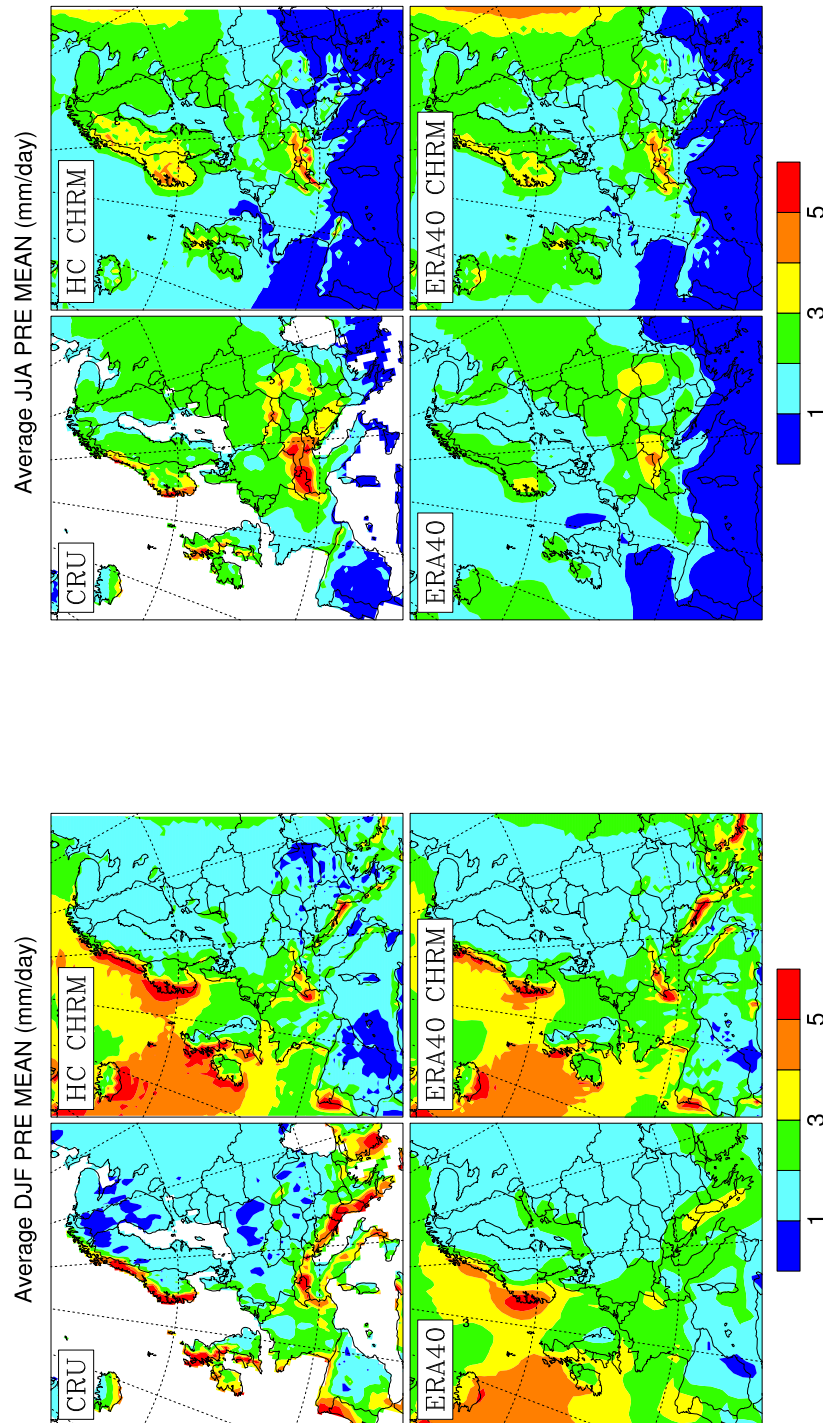


Figure 1. Mean 1961-1990 precipitation for winter (left) and summer (right) in mm/day. The four panels in each plot show CHRM simulations driven by the ERA-40 reanalysis (ERA40 CHRM) and the HC model chain (HC CHRM), along with an analysis of observational data (CRU), and results of a reanalysis (ERA40).

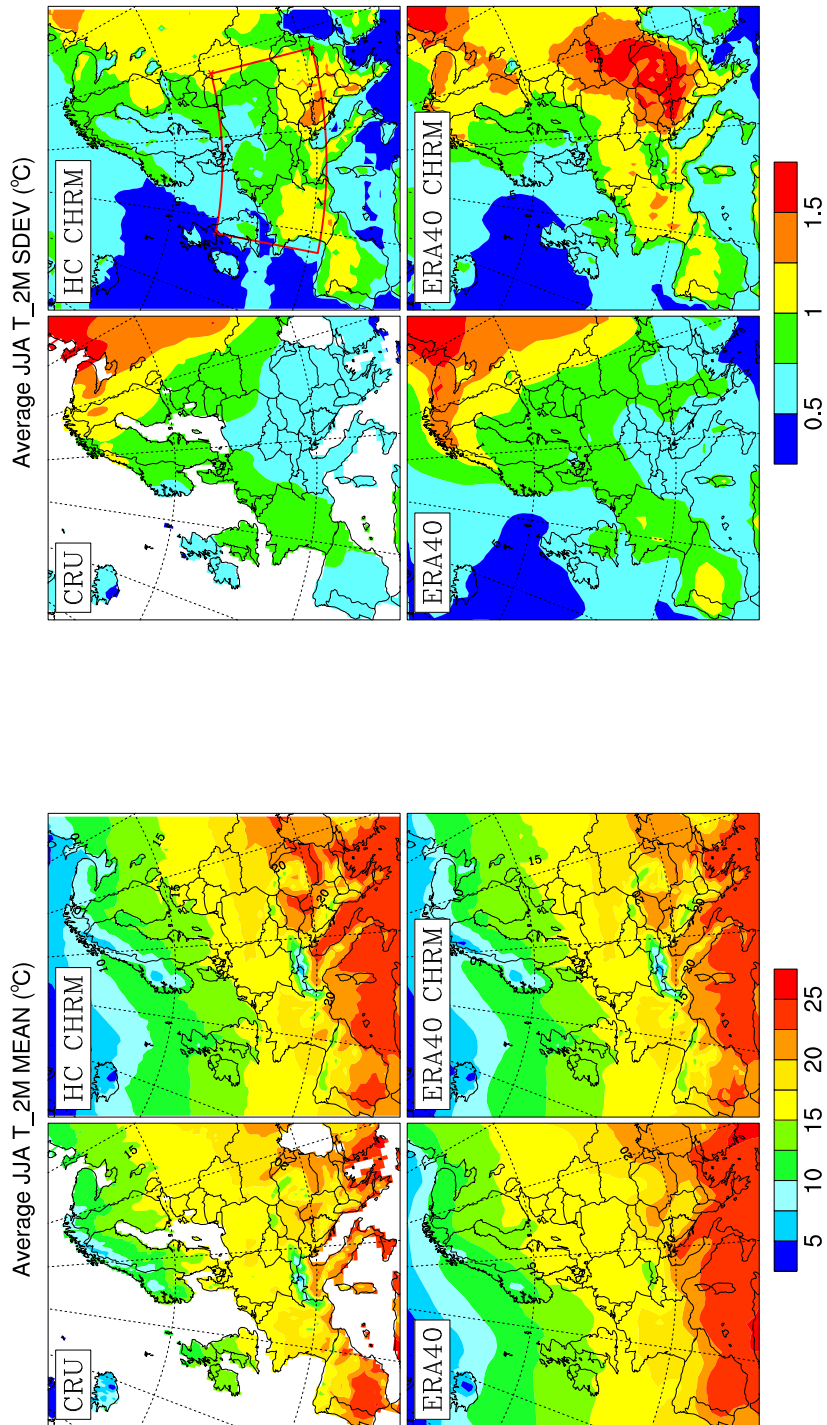


Figure 2. 1961-1990 summer temperature as simulated by CHRM: mean (left) and standard deviation (right), in °C. The four panels in each plot are as in Fig.1. The red box on the top-right panel defines the region used for area averaging in subsequent analysis (land points only).

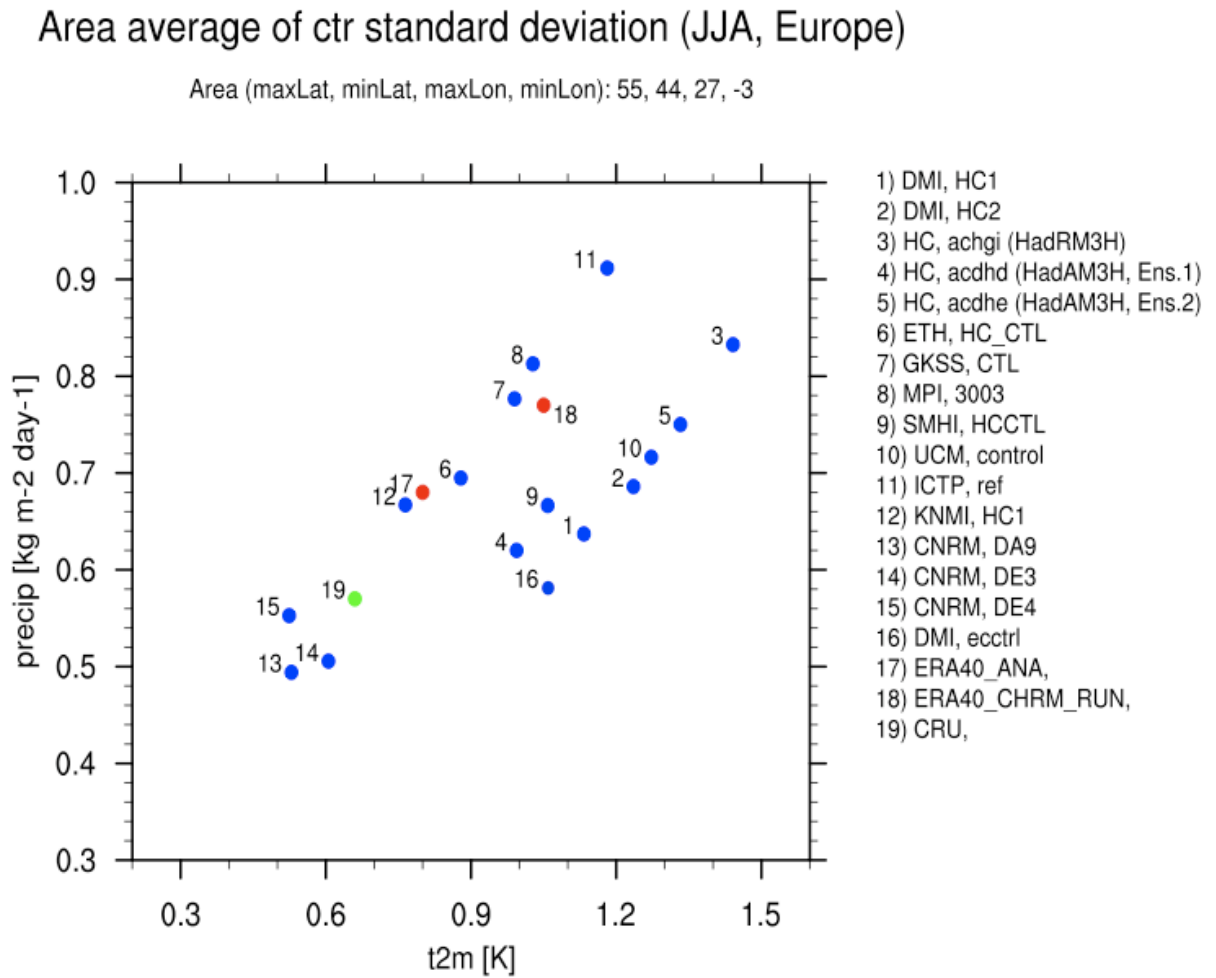


Figure 3. Comparison of variability as simulated by PRUDENCE models for 1961-1990. Blue data points show domain-averaged values of the standard deviation of precipitation and 2m temperature for Central Europe in mm/day and K. The averaging domain is shown in Fig. 2. The green data point shows the CRU observations, the red points show the ERA-40 reanalysis and a CHRM simulation driven by ERA-40.

t2m, ENS, (ctr), (scn)

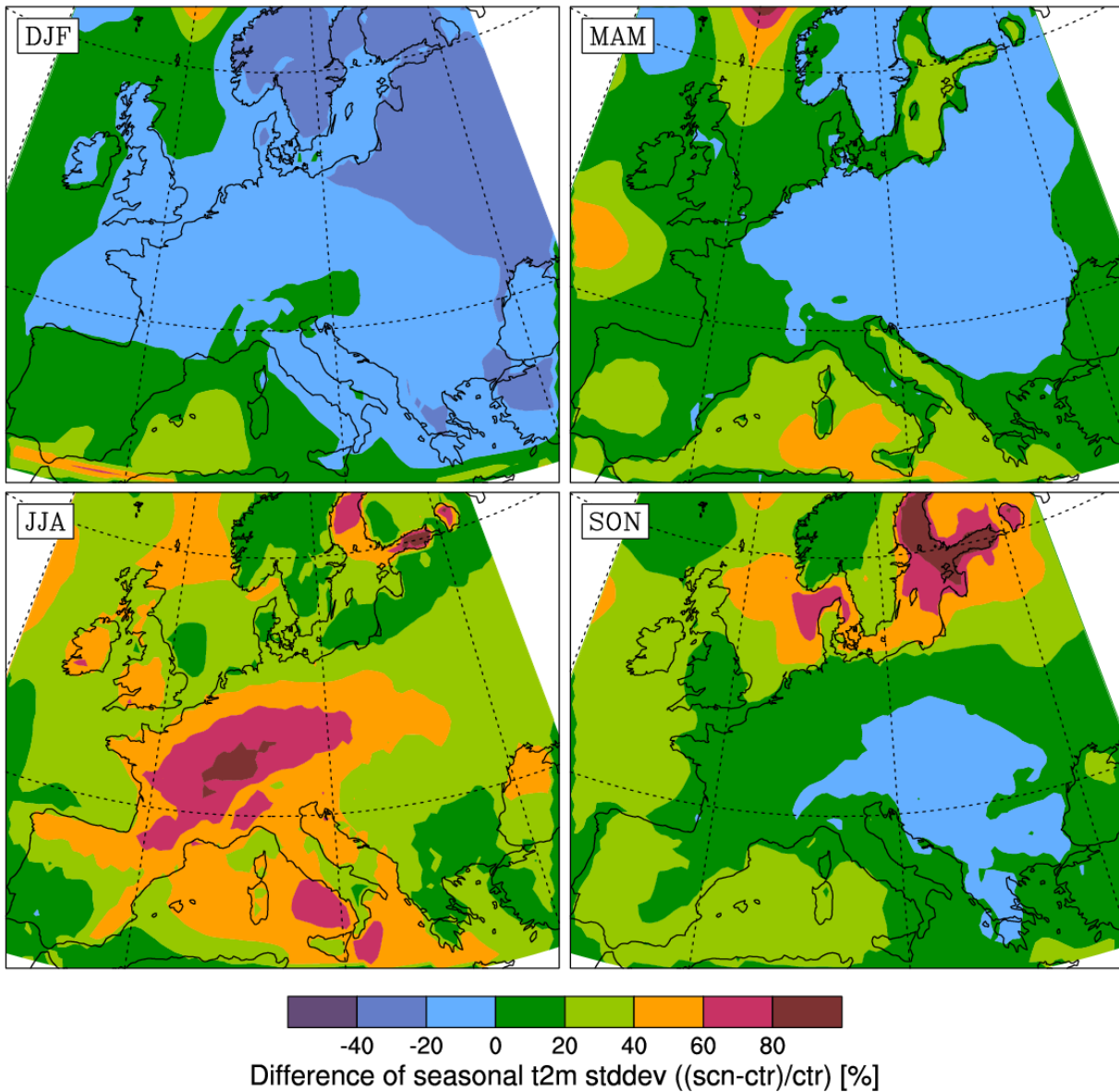
Data source, prudence.dmi.dk/private/index.html -> direct download/seasonal

Figure 4. Ensemble mean changes of the interannual variability of surface temperature for the four seasons, expressed as relative change $(SCN-CTL)/CTL$ of standard deviation in percent. All models in Table 1 are included.

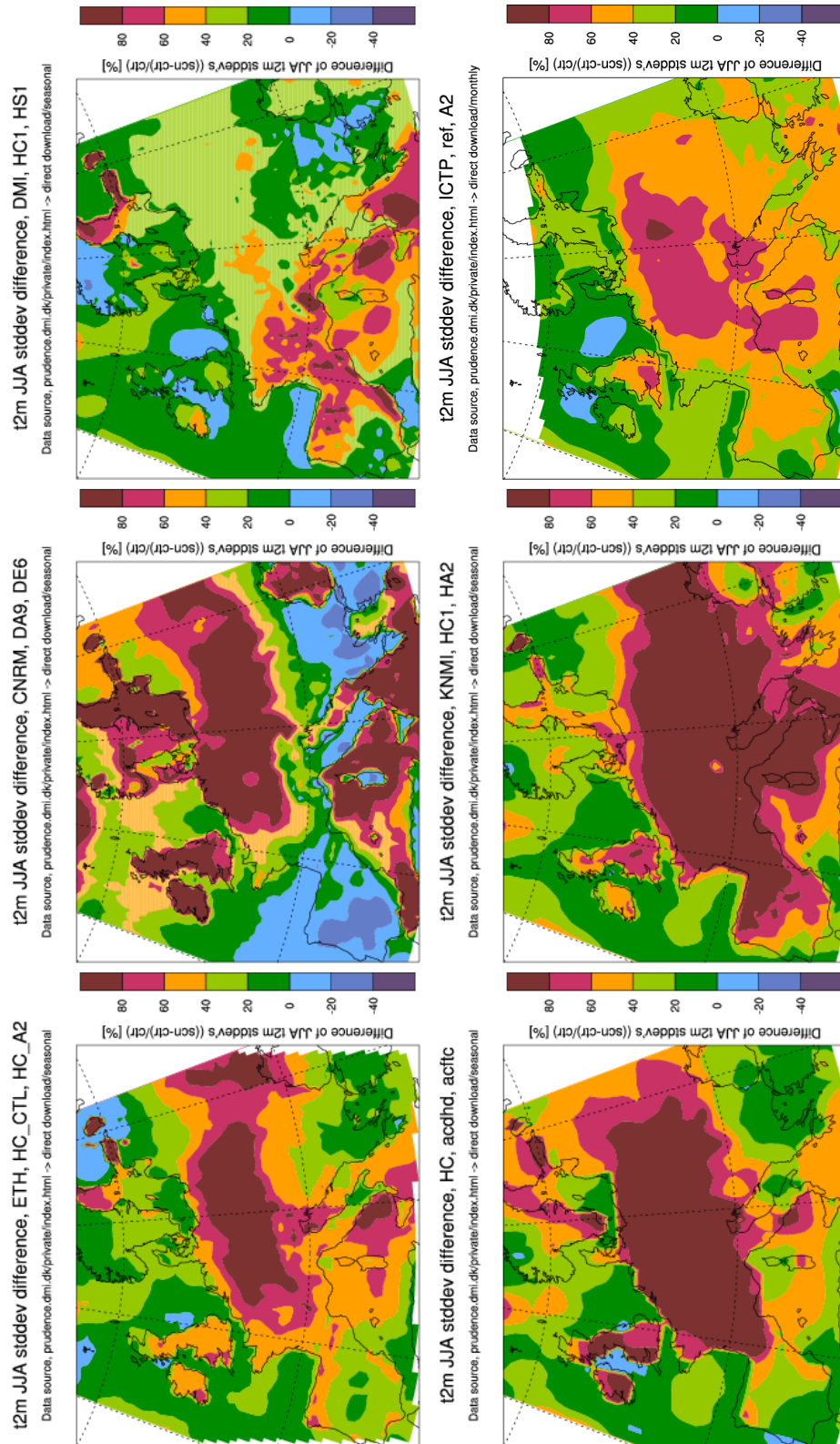


Figure 5. Changes in JJA interannual variability of surface temperature, expressed in percent. The panels show the results of six selected models/groups (from left to right and top to bottom): CHR/ETH, CNRM/MeteoFrance, HIRHAM/DMI, HadAM3/HC, RACMO2/KNMI, RegCM/ICTP.

Area average of standard deviations (JJA, Europe)

Area (maxLat, minLat, maxLon, minLon): 55, 44, 27, -3

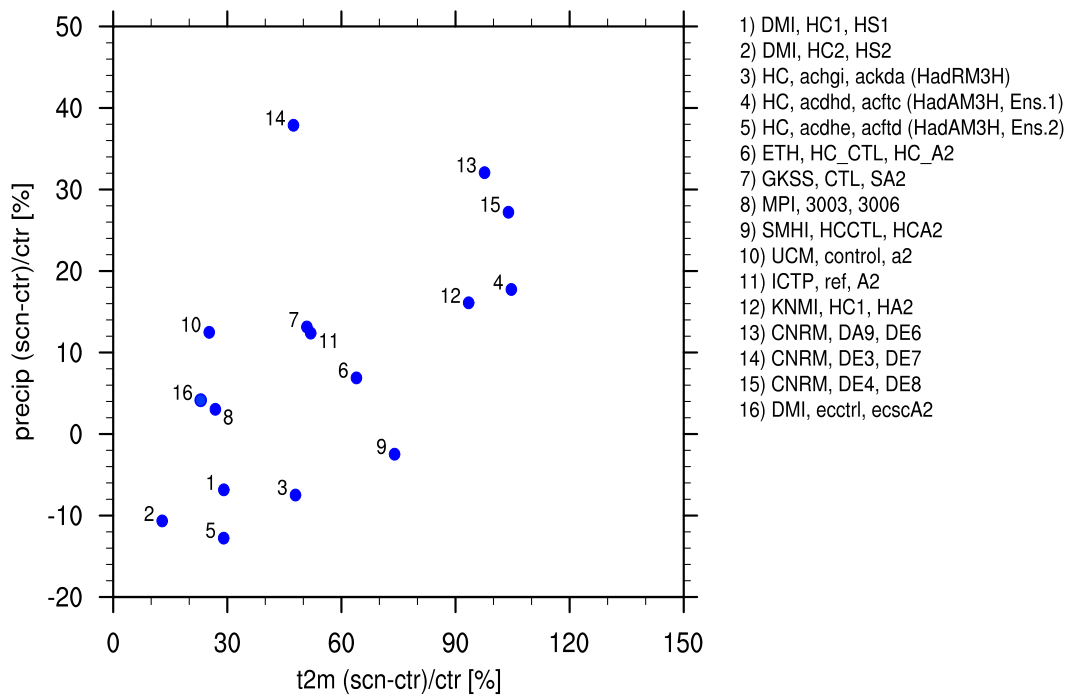


Figure 6. As in Fig. 3, but showing the variability changes as simulated by PRUDENCE models, in percent.

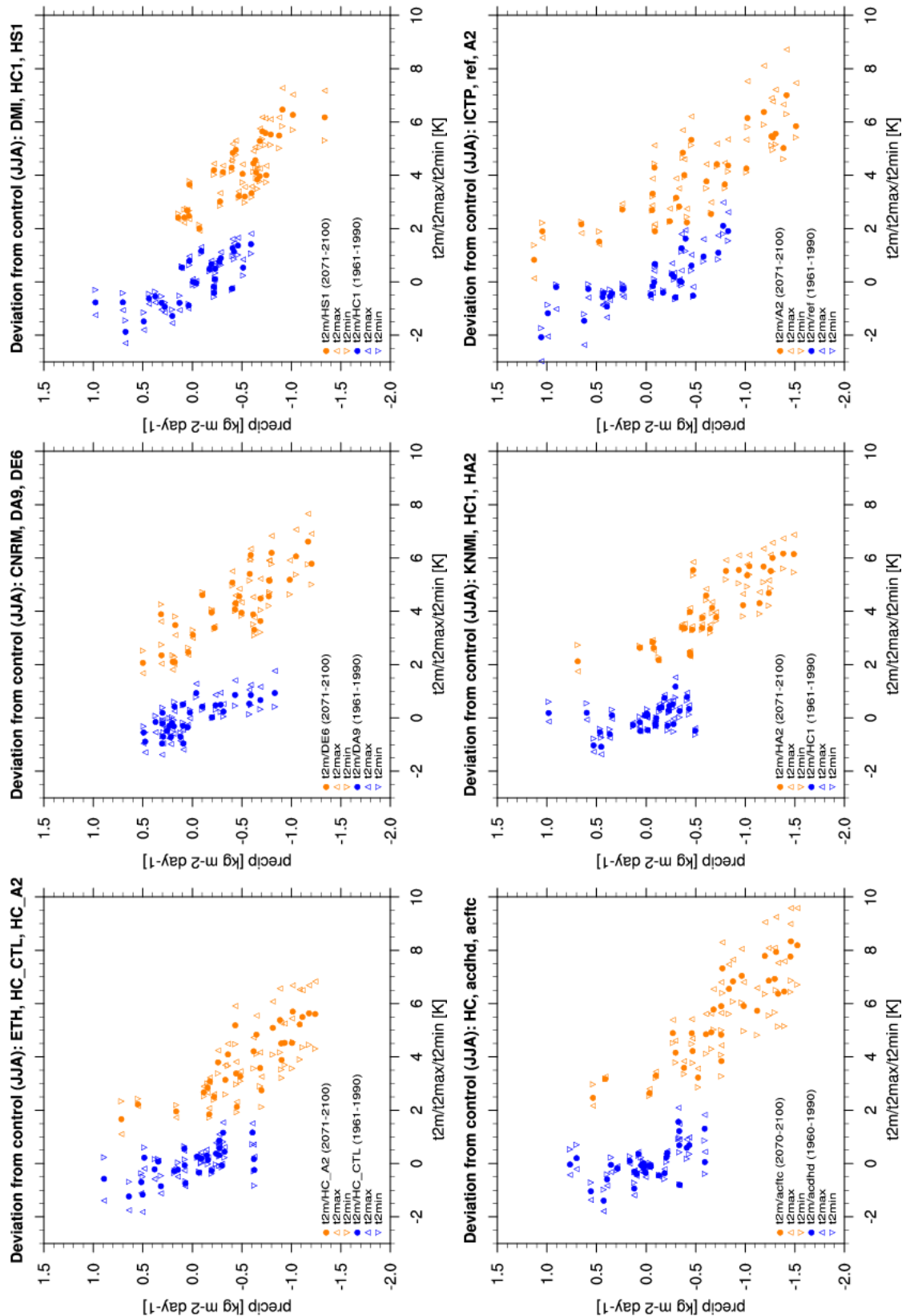


Figure 7. PRUDENCE simulated JJA temperature versus precipitation anomalies with respect to 1961-1990 means, for the same models as in Fig. 5, in K and mm/day. The three symbols show seasonal averages of minimum, mean and maximum temperatures.

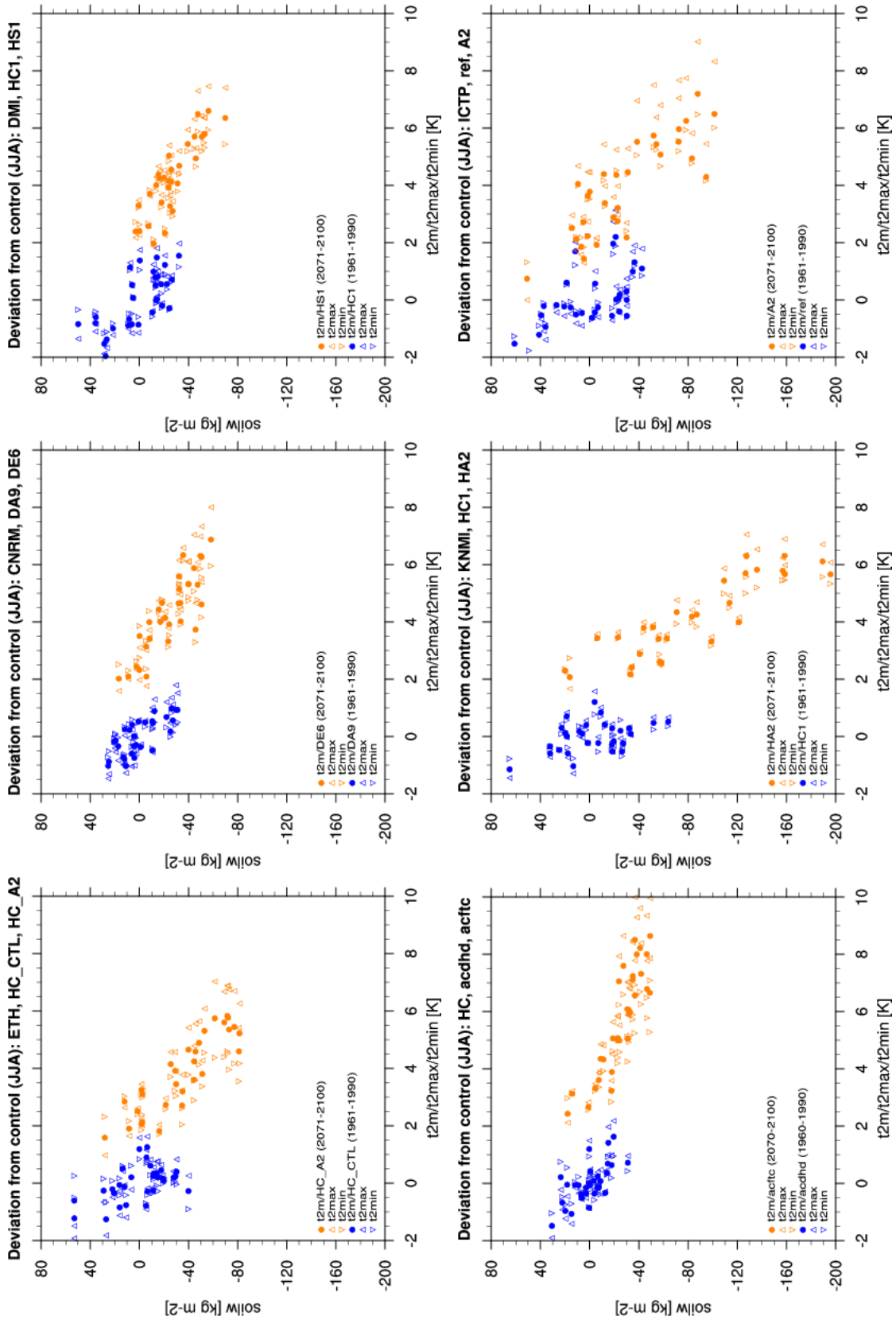


Figure 8. PRUDENCE simulated JJA temperature versus soil-moisture anomalies with respect to 1961-1990 means, for the same models as in Fig. 5, in K and mm.

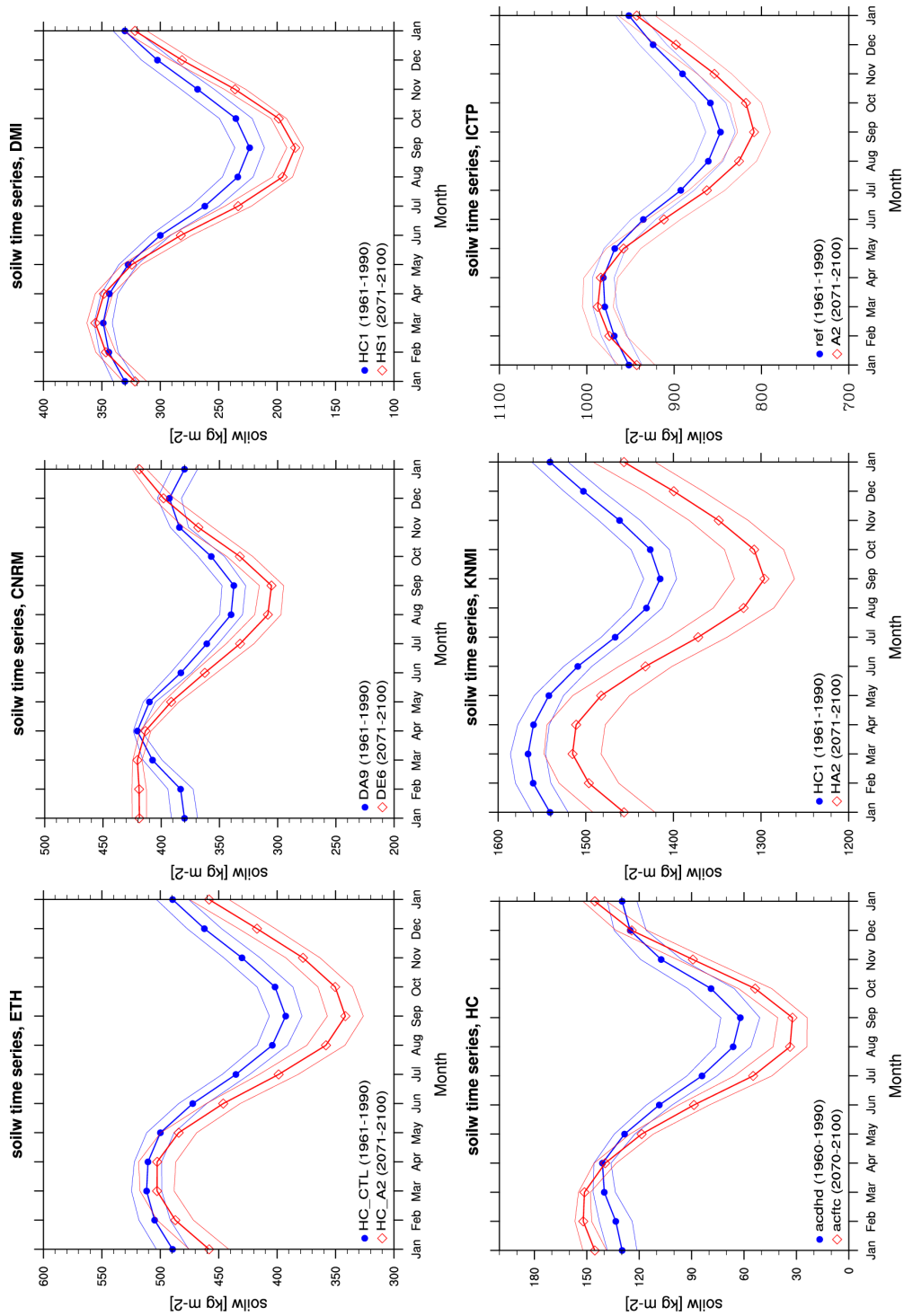


Figure 9. Mean yearly cycle of total soil moisture content in CTL (blue) and A2 scenario (red) experiments for the same models, as in Fig. 5, in mm. The thin lines above and under each thick line indicate the spread within the two 30-year periods, expressed in terms of the standard deviation.

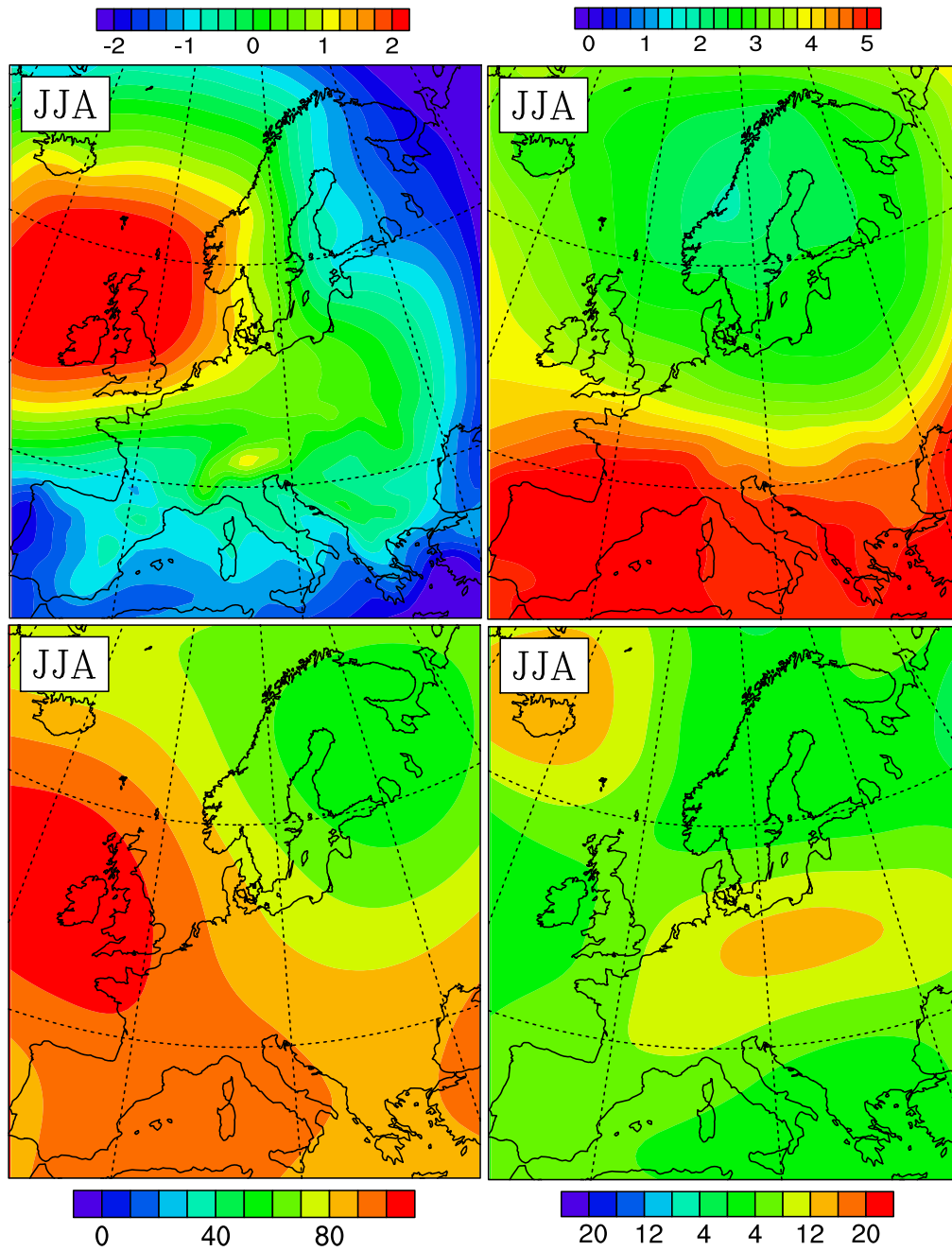


Figure 10. Changes in JJA synoptic-scale circulation, as simulated by the CHRM model (2071-2100 versus 1961-1990). Top left: change in mean MSL pressure (hPa); top right: change in mean 850hPa temperature (K); bottom left: change in mean 500 hPa height (m); bottom right: change in standard deviation of 500hPa height (m).